www.DeepakPublishing.com

Villafranca, A. et al.. (2012): JoSS, Vol. 1, No. 1, pp. 19-29
(Peer-reviewed article available at www.jossonline.com)

www.JoSSonline.com

Limitations of Hyperspectral Earth Observation on Small Satellites

Alberto G. Villafranca, Jordi Corbera, Francisco Martín And Juan Fernando Marchán

Programa Català d'Observació de la Terra - Institut Cartogràfic de Catalunya (PCOT/ICC), Barcelona, Spain

Abstract

Small satellites offer the means for a consolidated strategy for fast, economical access to space. Their role in national and regional programs is of great value in today's world, as they provide affordable means to obtain remote sensing data. This has proven to be especially useful for developing countries, many of which encompass large and remote expanses of territory. The high degree of development of small satellite technology facilitates increasing capabilities of onboard Earth Observation (EO) sensors. With missions already operating in the high resolution range (< 5 m) and several spectral bands, the performance of these sensors will be soon limited by the laws of physics. Newly envisaged small satellite missions include plans for an increasingly high number of bands – reaching up to hundreds of them – while maintaining good spatial resolution. This imposes a challenge in the coverage, the spatial resolution, and the quality of the data that can be obtained with these systems. In this paper, we analyze the restrictions facing hyperspectral sensors on small platforms caused by the limited volume and power available. The constraints imposed by the physics of optics on the signal-to-noise ratio (SNR) and the modulation transfer function (MTF) are also described, as well as the problems arising from the large amounts of data generated by such missions.

1. Introduction

Although hyperspectral sensors were originally developed for air platforms, spaceborne models are becoming increasingly frequent since the first operative hyperspectral sensor developed for the EO-1 mission (Pearlman et al., 2003). These sensors, typically offering several tens or even hundreds of spectral bands in the VNIR/SWIR/TIR regions, are capable of identifying Earth's soil components and estimating their abundance with a high degree of accuracy. Nevertheless, when adapting these sensors to the small satellite class, several problems arise. The analysis carried out in this article addresses spacecrafts of up to 100 Kg of total mass, thus belonging to the mini/microsatellite class.

Corresponding Authors: Alberto G. Villafranca - alberto.gonzalez@icc.cat and Jordi Corbera – jcorbera@icc.cat.

Within this class, problems appear when a high number of bands are to be obtained, because of the difficulty of splitting the continuous spectra that enter through the telescope aperture into narrow bands. Moreover, these bands may have to be routed towards sensors in different spatial locations, thereby increasing the complexity of the focal plane assembly.

Another issue arises when dealing with the quality of the gathered data. As the spectral bands are narrowed, the amount of energy conveyed by the photons becomes smaller. Consequently, the signal-to-noise ratio (SNR) decreases. The restricted size imposed on the sensor by the small satellite platform also affects the modulation transfer function (MTF). Finally, there is also a problem linked to the generation of the data. If significant territory areas are to be scanned with high spectral and spatial accuracy, high data volumes are generated. This poses a serious constraint on the communications system of the spacecraft.

The analysis developed in this article focuses on the quality of the data that can be obtained from a theoretical hyperspectral instrument and its limitations. The critical importance of data quality in EO missions has been seen in the work of the Institut Cartogràfic de Catalunya (ICC), the official mapping agency of the autonomous government of Catalonia (Spain), which is concerned with the generation of added-value geoinformation data, products and services. This institution has been operating its own airplanes (currently flying a Beechcraft B200, a Cessna Caravan 208B and a Partenavia P-68) and instruments (hyperspectral VNIR and TIR, digital high resolution camera, LIDAR, etc.) for almost 30 years. Our experience allows us to assert that from the point of view of both the final user and the generation of added-value products, the quality of the gathered data is essential.

Meanwhile, the Catalan Earth Observation Program (PCOT/ICC) is currently developing technical, economical and programmatic studies applied to MediMap, another mission for regional EO. MediMap is a small mission satellite under 100 Kg, with 6 bands in the VNIR region, and a hyperspectral secondary payload (Corbera et al., 2011). The main goal of this mission is to generate high-quality data to monitor changes in the region of Catalonia. MediMap has originated a detailed analysis of the potential hyperspectral capabilities of small satellite missions. Here, we present its results and conclusions.

In Section 2 of this paper, we perform an in-depth analysis of the limitations associated with the EO sensors onboard small satellites, and Section 3 addresses the data generation problem. Finally, in Section 4, we discuss the results of this study.

2. Quality Limitations of the Small Satellites

The main parameters influencing the image quality of EO sensors are the signal-to-noise ratio (SNR) and the modulation transfer function (MTF). The SNR is an intrinsic limiting factor in the intensity measurement using radiometry. On the other hand, the MTF represents the transfer quality of an optical system depending on the spatial frequency, providing the system response to the signal depending on its variation speed. Consequently, higher spatial frequencies are filtered through the system, resulting in blurry patterns in the image associated with these high frequencies. This study especially focuses on the optical limitations that arise from the miniaturization of the payloads.

2.1 Signal-to-Noise Ratio (SNR) Analysis

The SNR provides a statistical measurement of the resemblance of the incoming signal to the original one. Hence, it is an indirect indicator of the image quality at the instrument compared to the real one. SNR calculation is defined as $P_{signal} / P_{noise,}$ representing signal and noise power respectively.

The human eye can recognize well-defined patterns with SNR as low as 0.1, i.e., the signal power from the object is 10 times lower than the noise. However, for general purposes, acceptable quality requires an SNR > 10, while excellent quality is obtained when SNR > 40 (Holst et al., 2007). Nonetheless, the SNR specification for space imaging in most missions is typically around 100 and beyond, as reflected in the different small satellite missions analyzed in Sandau et al. (2010). Because hyperspectral applications require good quality to accurately differentiate among materials, we will set SNR = 100 as the minimum level for an operational mission.

Initially, in order to evaluate the signal power, a physical model of the EO system is required (Larson et al., 1999). There are two contributing sources of signal: Sun and Earth. We will focus on the visual and near infrared range (VNIR; 400-1000 nm), as it is the most representative region for most EO missions, including MediMap. Furthermore, in this range, the quality of the data obtained is better than in short-wave infrared range (SWIR; 1 – 2.5 μm) or in thermal infrared range (TIR; 8 – 12 μm), thus defining a best-case scenario. The Earth-generated signal in this range is negligible. The ground surface radiance is basically influenced by solar illumination, which has been simulated through the black body equation at T = 5900 ºK:

$$L_\lambda = \frac{\int E_\lambda}{4\pi}\alpha_P(1-L_{at})r_E =$$

$$= \frac{1}{4\pi}\int_{\lambda_{\min}}^{\lambda_{\max}} \frac{2\pi hc^2}{\lambda^5(e^{ch/kT\lambda}-1)} d\lambda \left(\frac{R_S}{d_{S-E}}\right)^2 (1-L_{at})r_E \qquad (1)$$

where E_λ is the spectral irradiance of the Sun, transformed to radiance by the 4π factor, αP is the propagation loss, L_{at} is the atmospheric absorption and r_E the reflectivity of the ground surface. We have used L_{at} = 0.2 and r_E = 0.3, which are typical values, as can be seen in Elachi et al. (2006) and Larson et al. (1999). From the radiance, the energy flux collected by the instrument (E_{opt}) can be calculated. Subsequently, the number of recovered photons (N_p) and generated electrons (e^-_{detec}) are obtained.

$$t_S = \frac{GSD}{V_g}; \quad A_{opt} = \pi\left(\frac{D_{opt}}{2}\right)^2 \qquad (2)$$

$$E_{opt} = \frac{A_{opt}}{h_{orb}^2} L_\lambda \cdot GSD^2 \cdot t_s(1-L_{at}) \qquad (3)$$

$$N_p = \frac{\lambda}{ch} E_{opt} \qquad (4)$$

$$e^-_{detec} = N_p \tau_{TX} \tau_{SP} \eta_Q \qquad (5)$$

where t_s is the pixel integration time, and A_{opt} is the recollection area or aperture. Finally, τ_{TX}, τ_{SP} and η_Q are, respectively, the optics and filters transmission coefficients, and the quantum efficiency of the detector. The adopted value for both transmission coefficients is 0.9, slightly higher than those of Schott (1997), to leave room for potential improvements in the technology. For the quantum efficiency we have also selected a value of 0.9, a near-perfect efficiency (Bass, 1995). Note than in these cases, little improvement margin is left, even when considering an ideal case.

At Equation (5), the signal level is obtained. The noise level must then be calculated to finally compute the SNR. There are two kinds of predominant noise to be considered at the detector: additive (or bias) noise and shot noise. Bias noise groups the detector intrinsic noise and the read-out noise, and it is dominant for photon-starved targets. On the other hand, shot noise is associated with the Poisson distribution of the photons' arrival, thus becoming dominant for bright targets, Nsh= $\sqrt{\text{e-}_{detec}}$. Although bias noise can be reduced (it is technology-dependent), there is no way to avoid shot noise (Schott, 1997). We will assume a good signal level; otherwise, the SNR obtained would not be representative of a nominal operation, i.e., of the instrument limitations. Hence, only shot noise will be significant in our model.

In the top panel of Figure 1, we plot irradiance and a merit figure of the SNR depending on the frequency. Note that there is a shift in the maximum position of both figures, due to the fact that the SNR depends here on the shot noise, i.e., the number of received photons. Although the energy for λ = 622 nm is lower with respect to the maximum at λ = 491 nm, the peak of the number of photons received is located in 622 nm, as their energy has also decreased.

To maintain a representative frequency analysis inside the whole VNIR range, we will choose a frequency presenting an intermediate SNR. The worst case is at 80% of the maximum SNR (located at 400 nm, top panel of Figure 1). Hence, an SNR = 90% of the maximum, e.g. 450 nm, is selected for the calculations where a fixed frequency is required. The bottom panel of Figure 1 represents the evolution of the ground sample distance (GSD) – the spacing of the ground area captured by each pixel – depending on the focal length and the pixel size. The bottom-right zone corresponds to the

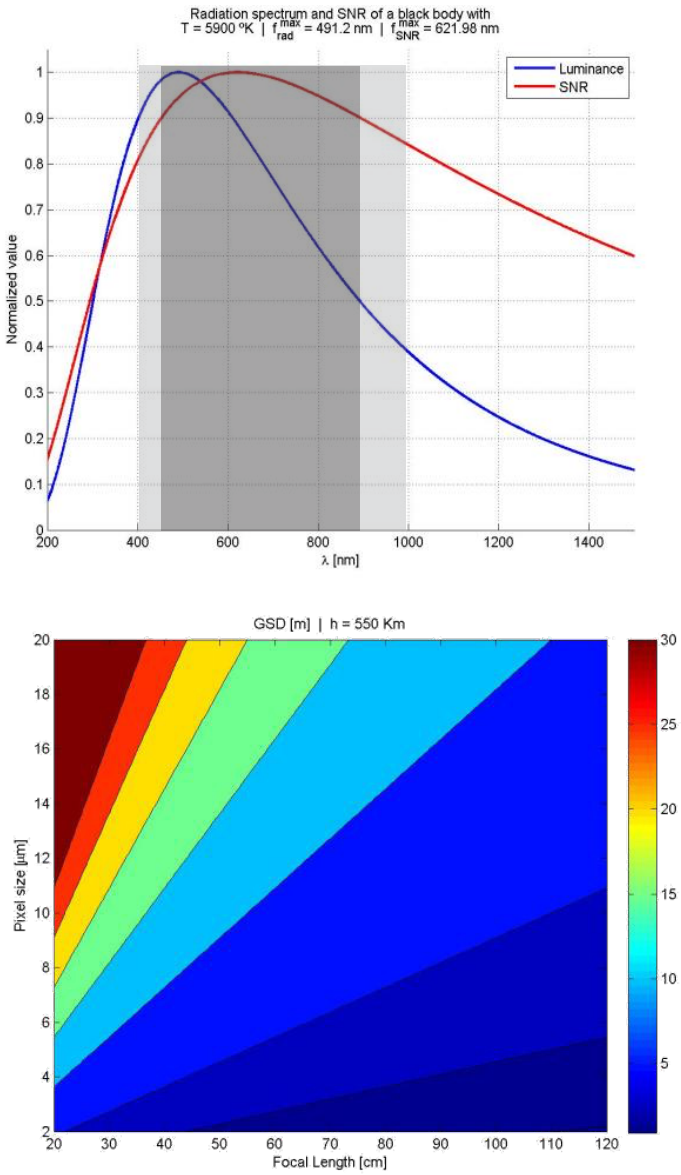

Figure 1. Top: Relative values for irradiance combined with a merit figure of the SNR. In grey, the VNIR interval, and in dark grey, the frequency interval presenting an SNR greater than the 90% of the maximum value. Bottom: GSD depending on the pixel size and the focal length for a LEO height of 550 Km.

sub-2.5 m resolution, the 1 m zone being adjusted to the bottom-right corner. The remaining boundaries correspond to 5, 10, 15, 20, 25, and 30 m. Values above 30 m have been grouped in the deep-red zone. Also note that the selected orbit height is constant at 550 Km during the whole study, which is a typical value for this kind of mission.

A standard value for the pixel pitch of the detectors used in space is currently in the range of 20 to 30 µm. This value allows a large collection area, but decreases the GSD for a given focal length when compared with smaller pitches. Nevertheless, one of the characteristics of small satellite technology is an intensive use of common off-the-shelf (COTS) components as a way of reducing costs. In MediMap, we have planned the use of a COTS detector (Corbera et al., 2011), representing an important cost reduction. A typical characteristic of these COTS sensors is a smaller pitch, currently ranging between 7 to 15 µm (Sandau et al., 2010). In this way, it is easy to obtain higher resolution in compact instruments, although one must be extremely careful with the radiation effects and the reduction of the incoming signal strength.

There are techniques that artificially allow the improvement of SNR values, namely, time-delayed integration (TDI) and forward motion compensation (FMC). Both techniques increase the number of photons received by the sensor, although they use different principles. TDI uses a row of pixels in the along-track direction that synchronously tracks the apparent motion of the pixel in the detector. Hence, if we have a 10-pixel row the amount of light gathered increases by a factor 10. FMC, on the other hand, slows the apparent pixel track in the detector through an accurate control of the satellite rotation. Usually, the satellite will point in the direction of the nadir. With FMC, this direction is modified to reduce the apparent ground speed. The ultimate effect of this technique is to increase the dwell or integration time. Unfortunately, as will be explained in the next section, these techniques set important constraints on the stability of the platform, and cannot be used to increase the integration time by a large factor (< ~32). Moreover, in the case of FMC, there is also a limiting constraint related to the variation of the spacecraft perspective during the capture. The most important noise in our system will be the shot noise, as has been previously explained. Consequently, the SNR increase will depend on the square root of the FMC or the TDI factor. Hence, SNR increases of a factor greater than ~ 5 or 6 do not seem feasible solely through the increase of FMC/TDI parameters.

Figure 2 (top) shows the dependence of the SNR with the GSD and the optics aperture. We consider the SNR requirement as 100, and a TDI/FMC system increasing the dwell time by a factor 16, i.e. the $SNR_0 = 4 \cdot SNR_i$. Also, the bandwidth selected is 10 nm, typical for hyperspectral measurements (Weng 2010, p. 101). For the range of apertures of a 100 Kg-class satellite (~20 cm), the amount of signal received is insufficient to reach the specified SNR for GSD < 6 m. Furthermore, the SNR rapidly decreases below this GSD, presenting an SNR < 10 at 3 m. Note the important effect on the quality, when reducing the GSD. Apart from the observed area shrinkage, we must also consider the reduction of the dwell time. Combined, these two factors ultimately cause a reduction of n^3 of the SNR when diminishing the GSD a factor n. The bottom panel of Figure 2 shows the low dependence of the SNR on the frequency variation.

In the top plot of Figure 3, the relation of the SNR with the bandwidth is analyzed. The SNR > 100 region (yellow) limits to 5 m the minimum GSD for $\Delta\lambda$ = 10 nm. Nonetheless, common values for multispectral missions such as $\Delta\lambda \sim 40 - 80$ nm (Weng 2010, p. 102) would allow to enter the sub-4 m region. On the

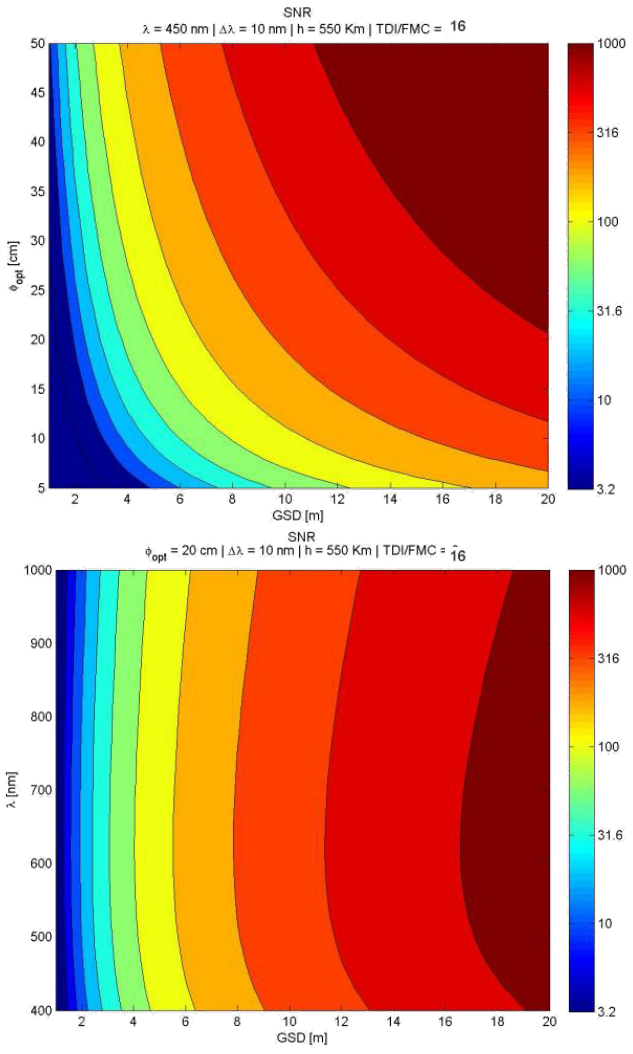

Figure 2. SNR depending on the GSD and the aperture diameter (top) or the GSD and the frequency (bottom) for typical values of bandwidth and height in an hyperspectral EO mission. In the figures, it is assumed that TDI/FMC techniques increase the dwell time in by a factor of 16.

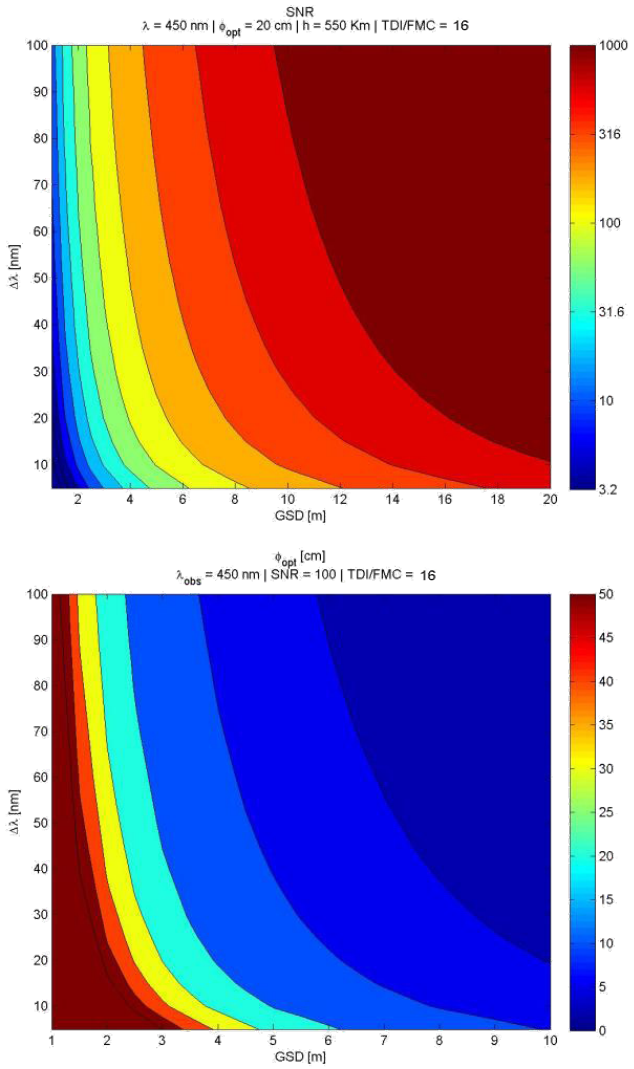

Figure 3. Top: SNR depending on the GSD and the bandwidth for typical values of aperture, frequency and height. Bottom: Minimum aperture diameter to obtain a SNR = 100 depending on the GSD and the bandwidth for a typical frequency. The dwell time has been artifically increased by a factor 16.

bottom panel of Figure 3, we have plotted the required aperture to achieve an SNR = 100. In this case, the interesting region would be the turquoise area. The blue regions correspond to apertures ø < 15 cm, ø < 10 cm, and ø < 5 cm, respectively. Note that for GSD > 10 m, it is theoretically possible to achieve hyperspectrality, i.e., narrow bandwidths, even for small apertures (ø < 10 cm). Unfortunately, it seems very difficult to go beyond the sub-3 m GSD for hyperspectral measurements, even with high dwell time increases by using TDI or FMC techniques and large apertures to increase the input signal. Consequently, the only way to achieve GSDs around 1 m for hyperspectral bandwidths (~10 nm) is with larger apertures. Hence, there is a need to provide small platforms with low-cost deployable mechanisms that will increase the light-collecting power of the sensors.

2.2 Modulation Transfer Function Analysis

The other relevant parameter to estimate the quality of an optical instrument is the MTF, an adimensional parameter determining the capacity of an optical system to transfer or capture the changes of the target. An optical system presents a low-frequency pass filter behavior, which results in blurry edges in the image. The frequency response of the system is measured by the MTF and is specified for a range of spatial frequencies. Nonetheless, typically only one value is specified for the sake of simplicity, corresponding to the Nyquist frequency of the instrument, i.e., half of the normalized spatial frequency. One of the advantages also given by the MTF model is the possibility of combining the MTF of the different separate elements to obtain the system MTF (MTF_{sys}). Considering only the most important factors affecting the MTF_{sys}, it can be defined as $MTF_{sys}=MTF_{optics}\cdot MTF_{D}\cdot MTF_{PS}$ as shown in Sandau (2006). The different MTFs stand for the optical system (including aberration and diffraction), the detector, and the platform stability, respectively.

In order to obtain the limitations of a given instrument, we will assume an aberration-free system, which currently, can be closely matched with configurations such as three- mirror anastigmatic or TMA (Sandau, 2006). Under this assumption, the instrument will be diffraction-limited, hence presenting an optical MTF described by:

$$MTF_{opt}(f_x)=\left|\frac{2}{\pi}\left(\arccos(K)-K\sqrt{1-K^2}\right)\right|;\ K=\lambda\cdot F\cdot f_x\le 1 \quad (6)$$

where λ is the average wavelength of the radiation, F is the f-number (f/D), and fx is the spatial frequency in the x direction. This MTF is caused by the Airy disc. A good compromise solution is to make the diameter of the Airy disk *(ø = 2.44·λ·N)* of roughly the same size of the detector pixel pitch. In the top panel of Figure 4, we show the resulting MTF of the optical system at the Nyquist frequency depending on the pixel size and the f-number.

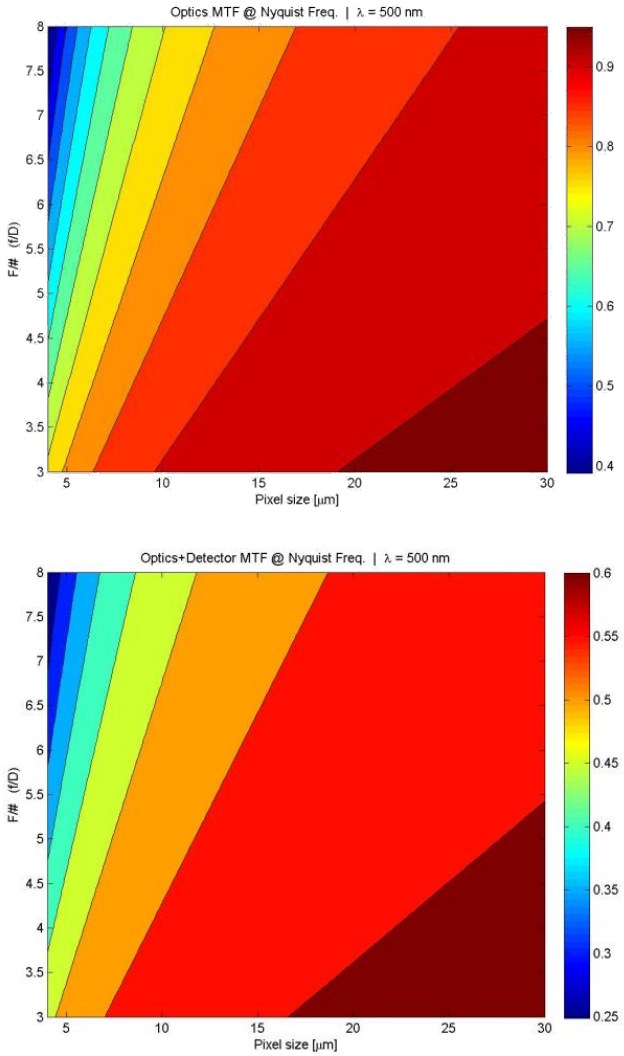

Figure 4. MTF of the optical (top) and optical plus detector (bottom) systems depending on the pixel size and the f-number. Note that the color bar scales are different in each case.

On the other hand, we know that the detector MTF is defined as

$$MTF_D(f_x) = \left| \frac{\sin(\pi \cdot d \cdot f_x)}{\pi \cdot d \cdot f_x} \right| \quad (7)$$

with *d* as the pixel size. The Nyquist frequency is defined as *1/2d,* thus fixing the value for the MTF_D to 0.64, no matter what the pixel size. When combined with the MTF_{opt},we obtain the MTF_{sys} for a perfect stabilized platform (bottom panel of Figure 4). As previously explained, the MTFsys must be as large as possible to deliver quality data. Therefore, we have interest in selecting the largest pixel pitch and the shorter focal length that allow the system to comply with performance specifications. Consequently, the GSD will increase, provided that the aperture diameter is constant. In other words, a system with a smaller GSD implies either a smaller pixel pitch or a larger focal length (or both), thus decreasing the MTF_{sys} and reducing their quality.

Nevertheless, as explained above, the pointing stability (PS) of the platform is also an important factor influencing the quality of the data. The PS can be separated into three different components: $MTF_{PS} = MTF_{LM} \cdot MTF_J \cdot MTF_{sin}$, representing linear motion, jitter, and sinoidal vibration (Sandau, 2006). The linear motion only affects the along-track direction of the satellite, and is related to the dwell time or integration time. Its associated MTF is defined as:

$$MTF_{LM}(f_x) = \left| \frac{\sin(\pi \cdot a_{LM} \cdot f_x)}{\pi \cdot a_{LM} \cdot f_x} \right| \quad (8)$$

where a_{LM} represents the distance the target moves across the detector pixel. Hence, when $a_{LM} = d$, the MTF associated with the linear motion is the same as the detector one. This effect is the reason why the dwell time can not be indefinitely increased, as it implies a proportional increase of this a_{LM} parameter.

The jitter or random noise aggregates different motions of the satellite (Schroeder, 2000), thus resulting in a Gaussian-distributed effective motion:

$$MTF_J(f_x) = \exp(-2\pi\sigma_J^2 f_X^2) \quad (9)$$

where σ_J is the rms random displacement of the target at the detector.

Finally, the sinoidal vibration is only important for systems with large integration times. When estimating the limitations of high resolution instruments, the integration times must be small to reduce the MTF_{LM}, thus presenting a negligible MTF_{sin} (Sandau, 2009). MTF_{sin} is associated with the sinoidal vibrations of the platform. However, TDI or FMC may also increase the importance of this effect to a non-negligible level. In this case, it should be included in the MTF_{PS} calculation.

In Figure 5, we show the resulting MTF when superimposing both linear motion and jitter. As we look for a good performance, the effect on the MTF_{sys} must be minimized. We will consider that an MTF_{PS} higher than 0.9 does not have an important effect in the system. Hence, only the bottom-left red region will suit this condition. Assuming intermediate values for both effects, we can affirm that provided that $a_{LM} < 0.3$ and $\sigma_J < 0.1$, the MTF_{sys} reduction is minimal. For high resolution missions, this implies a control of the stability below the arcsec/sec range.

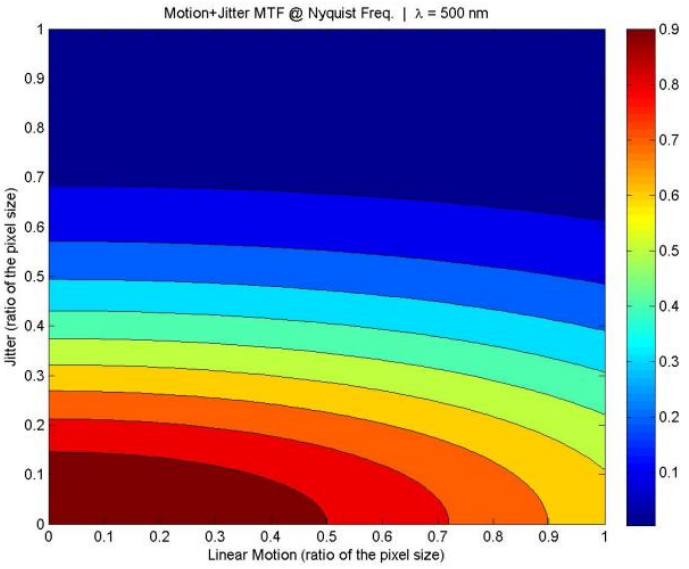

Figure 5. MTF caused by the linear plus the jitter movements depending on their different amplitudes.

Figure 6 shows the system MTF for different configurations. We can consider an $MTF_{sys} > 0.2$ as good, and $0.1 < MTF_{sys} < 0.2$ as fair (Sandau et al., 2008; Sandau et al., 2010). Below this level, the quality of the data rapidly degrades. The RapidEye mission can be used as a reference, as it currently represents an advanced small satellite on EO. RapidEye is a high-resolution commercial constellation of five identical satellites that must provide customers with high-quality data. Although it initially targeted an along-track $MTF_{sys} \geq 0.25$, the measurements performed in orbit revealed that there were large differences among the different satellites. Specifically, the red-edge band of satellites 2 and 4 feature an MTF_{sys} of 0.09, while satellite 5 presents an $MTF_{sys} = 0.30$ (Brunn et al., 2009). This proves the difficulty of designing the MTF of a high precision optical system, as it is subjected to high levels of mechanical and thermal stresses during the launch and the orbital operation. So it is important to keep in mind a security margin to compensate for unexpected effects. Moreover, the real instrument would suffer from additional effects, further reducing the MTF estimated here (Boreman, 2001).

The top plot of Figure 6 shows that for the calculated range, all the interval of F and pixel sizes guarantee an $MTF_{sys} > 0.2$. We have also added a small sinoidal effect, for a more realistic result. The lowest MTF (top-left corner) is 0.22. Note that the MTF decreases exponentially for low pixel sizes. Therefore, for pitches around 4 μm and high *Fs* we can no longer guarantee excellent performance. Moreover, due to this rapid degradation, when reducing the pixel size further, the quality of the data captured will be seriously compromised, even for small *Fs*.

The bottom panel of Figure 6 shows the effect of linear and jitter components as the two most important disturbing motions in the MTF_{sys} for what could be a state-of-the-art system configuration. With a 20 cm aperture, f = 1.1 m, and a height of 550 Km, it would deliver a GSD of 2 m. The boundary between yellow and blue delimits the $MTF_{sys} = 0.2$ region. To increase the integration time of the small pixels, the linear motion must be as large as possible, which at the same time tightens the jitter constraint ($\sigma_J = 0.2$ roughly results in 0.2 arcsec for the prior example). This is a best-case

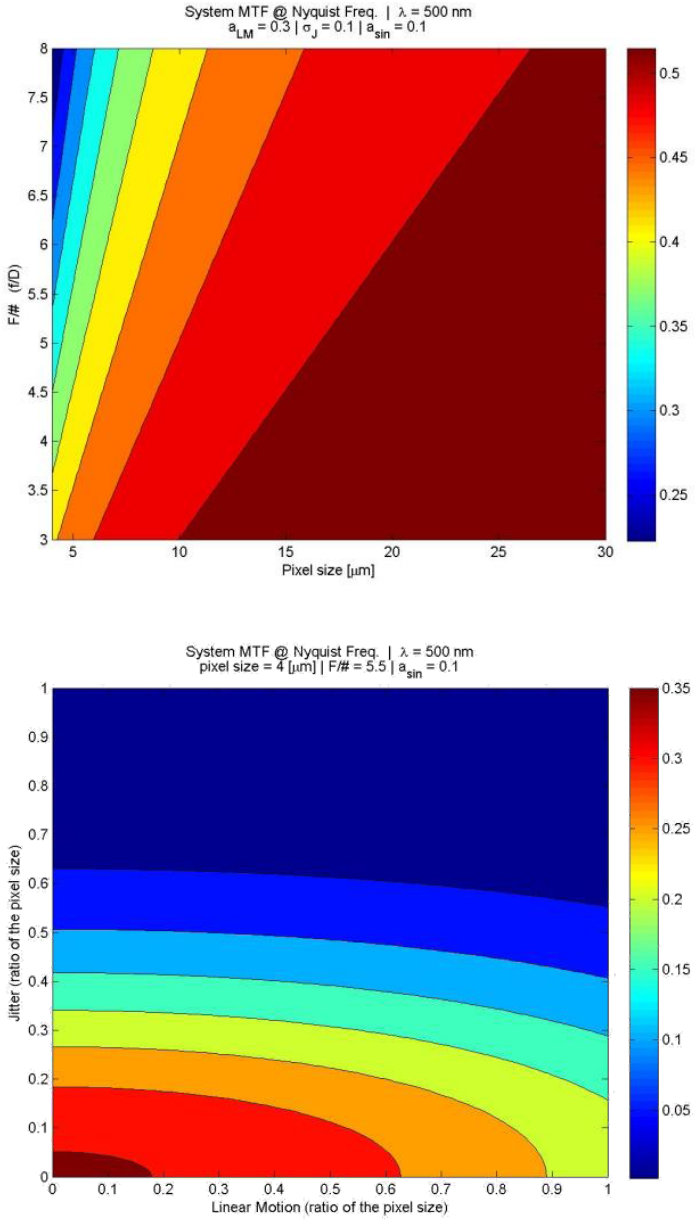

Figure 6. Top: MTF of the complete system with fixed linear + jitter + sinoidal components affecting the stability depending on the pixel pitch and f-number. Bottom: A similar case, this time with fixed pixel pitch, F – (f/D) – and sinoidal coefficient, depending on the linear motion and jitter amplitudes. Note that the color bar scales are different.

approximation; the final MTF_{sys} will always present a lower value.

Finally, it is important not to forget that both the SNR and the MTF influence the image quality, which is paramount to deliver quality geoinformation products and services. Both parameters must be optimized, if we are to obtain the best performance of a system. For ex-

ample, the system proposed in the previous paragraph would generate around 70 electrons/pixel (also with the assumptions made in Section 2.1) with $a_{LM} = 1$ (i.e. a large dwell time equal to the entire pixel transit time). This implies that the SNR < $\sqrt{70} = 8.2$. If a small value of bias noise is included (20 e^-/pixel), then the SNR ~ 3. Even if a large TDI of 32 stages is considered, the maximum theoretical SNR would be 46. Furthermore, the high a_{LM} limits the best possible MTF_{sys} ~ 0.2, even when $\sigma_J \rightarrow 0$. Therefore, we can see that the design of an optical system implies trading-off most of its parameters to obtain the best solution.

3. Data Volume Constraints

Data compression in hyperspectral missions is mandatory. It is possible to obtain sensible telemetry gains by adding some complexity to the system, which at the same time increases the power consumption. Specifically, current studies estimate that it is realistic to consider scenarios presenting an average information of 5 bits/pixel for lossless, 3 bits/pixel for near-lossless and 1 bit/pixel for lossy compressions (Magli et al., 2004; Ponomarenko et al., 2007; Ryan et al., 1997). Considering that most current detectors work with 12 or 14 bit/pixel quantization, the compression ratios may range from 2.4 to 14.

Nowadays, X-band links of 100 Mbps are becoming mainstream for many EO small satellites. Experimental links reaching up to 1 Gbps are being currently developed for small satellites. Using a 100 Mbps, a typical small satellite mission can download around 30 Gbyte/day with a polar station, i.e. 0.3 Tbyte/day with a 1 Gbps link (Corbera et al., 2011). A 1-m/100-band hyperspectral high-resolution small satellite would generate roughly 150 Mbytes/Km^2 without compression. This implies that an experimental 1 Gbps link can download 2000 Km^2/day, e.g. a square of only 45-Km side (14 Km using a 100 Mbps standard link). The number of Km^2 can be increased with compression, but a ratio larger than 4 is not advised, if data quality is to be maintained.

The amount of data generated by hyperspectral missions is growing exponentially, presenting a serious constraint for the extension of the scanned area. In order to mitigate this problem, different solutions can be used, such as extending the contact to other ground stations, or duplicating the link. However, these solutions pose budgetary and technical problems. For example, in both cases, larger amounts of energy will be required by the communication system of the spacecraft, thus increasing its complexity.

4. Discussion

The combination of a good SNR and MTF for a high-resolution instrument is extremely difficult, especially when dealing with hyperspectrality in a small platform. This poses a challenge for the miniaturization of this technology, which must lay the foundations of the new generation of small satellite instruments. Because these satellites benefit from the piggy-back launch slots offered by some launch providers, they have tight constraints in mass and size. The aperture size is initially clearly limited in the current technology, together with the maximum physical dimensions (i.e., focal length) and mass. Considering a typical aperture size of 20 cm, we have shown that it seems difficult to reach hyperspectrality with SNR > 100 for GSD < 5 m, even if we artificially increase the dwell time by a large factor with TDI or FMC. The narrow bandwidth required by the hyperspectral measurements limits the amount of light that can be gathered for each channel. Hence, an easy way to reduce the constraints would be to increase the bandwidth. This is currently applied by most EO missions, which typically feature between 4 and 10 bands. The key to go beyond this barrier may lie in deployable mechanisms that allow increasing the physical dimensions in space while keeping a low volume during the launching phase (Segert et al., 2006).

The MTF of the system (MTF_{sys}), also a key parameter in an optical system, depends on spatial frequency. However, usually, only the corresponding value at the Nyquist frequency is given. There is interest in using large pixels to reduce the MTF constraints, but this reduces the GSD of the system, as well. We have shown that the most important contribution to this MTF_{sys} comes from the detector, the optics, and the platform stability. The former is fixed to 0.64 and sets the maximum limit for a given detector. The contribution of the optical system is assumed to be attributable to the dif-

fraction of the system, and depends on the pixel size and the f-number. Finally, the platform stability demands an accurate control of the pointing while capturing images. Otherwise, the undesired motion of the platform will increase the MTF_{sys}, producing blurry images. In general, motion values during the dwell time lower than 30 % of the pixel size for linear motion and 10 % for the jitter produce a negligible effect on the MTF_{sys}. An example is shown in which a very compact instrument delivers 2 m GSD with $MTF_{sys} > 0.2$. However, there is clear interdependence of the SNR and the MTF with some of the system parameters — namely, the focal length, aperture, mission height, and detector pixel size.

Finally, the high volume of data generated by a high spatial and frequency resolution instrument presents an engineering challenge. Although compression helps to mitigate the problem, compression ratios beyond 5 or so are not recommended, as they imply the loss of sensible information. Consequently, only areas in the order of ~1000 Km^2/day would be scanned, even in the case of using experimental high-speed data links that are not yet commercialized. The use of several ground stations to increase contact times with the spacecraft would be the most feasible solution to deal with this problem.

High resolution hyperspectrality in small satellites of around 100 Kg seems feasible. An instrument with several tens of bands in the VNIR range, ~ 20 cm of aperture delivering 2 m of resolution has been analyzed. The SNR sets up the tightest restriction when entering the high-resolution/hyperspectral boundary. Nevertheless, the combination of high stability platforms and TDI or FMC mechanisms will increase the dwell time (i.e., SNR), without degrading the image quality. These results show that small platforms are capable of delivering EO data that matches the tight requirements of regional environmental and territorial challenges. As these platforms become real and affordable, their combination with compact hyperspectral instruments will allow the construction of EO constellations, delivering high-quality hyperspectral data with fast response at an affordable price.

References

Bass, M., et al. (1995): *Handbook of Optics: Vol. II*. New York: McGraw-Hill.

Boreman, G. D. (2001): *Modulation Transfer Function In Optical and Electro-Optical Systems*. Bellingham, WA: SPIE Press.

Brunn, A., et al. (2009): The RapidEye Calibration Approach and Current Results, presented at JACIE 2009, Washington, D.C. Available: http://calval.cr.usgs.gov/JACIE_files/JACIE09/TuesdayPM/WeicheltRapidEye.pdf

Corbera, J., et al. (2011): Boosting Small Satellites Missions for Earth Observation at Regional Level: Main Drivers and Experiences. S*mall Satellites for Earth Observation,* vol. VII, pp. 247-250. Berlin: Wissenschaft und Technik Verlag.

Elachi, C. and Van Zyl, J. (2006): *Introduction to the Physics and Techniques of Remote Sensing*. New Jersey: Wiley.

Guelman, M. and Ortenberg, F. (2009): Small Satellite's Role in Future Hyperspectral Earth Observation Missions. *Acta Astronautica*, vol. 64, pp. 1252-1263. Netherlands: Elsevier.

Holst, G. C. and Lomheim, T. S. (2007): *CMOS/CCD Sensors and Camera Systems.* Bellingham, WA: JCD Publishing/SPIE Press.

Larson, W. J. and Wertz, J. R. (1999): *Space Mission Analysis and Design: Vol.8*. Space Technology Library (3rd ed.). New York: Springer.

Magli, E., Olmo, G. and Quacchio, E. (2004): Optimized Onboard Lossless and Near-lossless Compression of Hyperspectral Data Using CALIC. *Geoscience and Remote Sensing Letters*, IEEE, vol. 1 (1), pp. 21- 25.

Pearlman, J.S., et al. (2003): Hyperion: A Space-based Imaging Spectrometer. *IEEE Trans. Geosci. Remote Sens*., vol. 41 (6), pp. 1160–1173.

Ponomarenko, N.N., et al. (2007): An Automatic Approach to Lossy Compression of AVIRIS Images. *Geoscience and Remote Sensing Symposium,* IGARSS 2007, IEEE International, pp. 472-475.

Ryan, M. J., and Arnold, J.F. (1997): The Lossless Compression of AVIRIS Images by Vector Quantization. IEEE Trans. *Geosci. Remote Sens.*, vol 35 (3), pp. 546-550.

Sandau, R. (2006): Potential and Shortcoming of Small Satellite for Topographic Mapping, in *Proc. ISPRS Workshop: Topographic Mapping from Space (with special emphasis on small satellites)*, ISPRS Vol. XXXVI-1/W41, Ankara, Turkey, 14–16 February 2006.

Sandau, R. (2009): System Considerations and Potential for Topographic Mapping with Small Satellites., in *Proc. ISPRS Workshop: High-Resolution Earth Imaging for Geospatial Information,* ISPRS Vol. XXXVIII, Hannover, Germany.

Sandau, R., et al. (2008): *Small Satellite Missions for Earth Observation: Selected Contributions. Heidelberg,* Germany: Springer.

Sandau, R., et al. (2010): *Small Satellite Missions for Earth Observation: New Developments and Trends.* Heidelberg, Germany: Springer.

Segert, T., et al. (2003): The Dobson Space Telescope – A Time-shared Telescope for NEO and Earth Observation, presented at the 4th International IAA Symposium on Small Satellites for Earth Observation, Berlin, Germany, Paper IAA-B4-0605.

Schott, J. R. (1997): *Remote Sensing: The Image Chain Approach.* New York: Oxford Univ. Press.

Schroeder, D. J. (2000): *Astronomical Optics*. San Diego, CA: Academic Press.

Weng, Q. (2010): *Advances in Environmental Remote Sensing: Sensors, Algorithms, and Application: Vol. 7.* Taylor & Francis Series in Remote Sensing Applications. Boca Raton, FL: CRC Press.